Journal of Solid State Chemistry 183 (2010) 385–391

Contents lists available at ScienceDirect

Journal of Solid State Chemistry

journal homepage: www.elsevier.com/locate/jssc

Fabrication and electron transport properties of epitaxial films of electron-doped $12CaO \cdot 7Al_2O_3$ and $12SrO \cdot 7Al_2O_3$

Masashi Miyakawa [a,*,1], Hidenori Hiramatsu [a], Toshio Kamiya [b], Masahiro Hirano [a], Hideo Hosono [a,b]

[a] Frontier Research Center, Tokyo Institute of Technology, Mail Box S2-13, 4259 Nagatsuta, Midori-ku, Yokohama 226-8503, Japan
[b] Materials and Structures Laboratory, Tokyo Institute of Technology, Mail Box R3-1, 4259 Nagatsuta, Midori-ku, Yokohama 226-8503, Japan

ARTICLE INFO

Article history:
Received 20 August 2009
Received in revised form
23 November 2009
Accepted 30 November 2009
Available online 5 December 2009

Keywords:
Epitaxial growth
Electron doping
Pulsed laser deposition

ABSTRACT

Epitaxial growth and electron doping of $12CaO \cdot 7Al_2O_3$ (C12A7) and $12SrO \cdot 7Al_2O_3$ (S12A7) are reported. The C12A7 films were prepared on $Y_3Al_5O_{12}$ (YAG) single-crystal substrates by pulsed laser deposition at room temperature and subsequent thermal crystallization. X-ray diffraction patterns revealed the films were grown epitaxially with the orientation relationship of (001)[100] C12A7 || (001)[100] YAG. For S12A7, pseudo-homoepitaxial growth was attained on the C12A7 epitaxial layer. Upon electron doping, metallic conduction was achieved in the C12A7 film and the S12A7/C12A7 double-layered films. Analyses of optical absorption spectra for the S12A7/C12A7 films provided the densities of free electrons in each layer separately. Hall measurements exhibited larger electron mobility in the S12A7/C12A7 film than those in C12A7 and S12A7 films, suggesting free electrons may be accumulated at the S12A7/C12A7 interface due presumably to a discontinuity of the cage conduction bands.

1. Introduction

The $12CaO \cdot 7Al_2O_3$ (C12A7) is used as a constituent of alumina cement [1–7] and is a good electrical insulator due to its large bandgap >6 eV [8]. Due to the large bandgap, it has been thought that C12A7 may be used only as an electronically passive material. In 2003, we found that C12A7 exhibits several active functionalities [9–11] by electron doping, which is achieved owing to its unique crystal structure [12]. The crystal lattice of C12A7 belongs to the cubic space group *I*-43*d* (No. 220). The unit cell has a lattice parameter of 1.199 nm and the chemical unit of $Ca_{24}Al_{28}O_{66}$, which is composed of a positively charged lattice framework expressed as $[Ca_{24}Al_{28}O_{64}]^{4+}$, which involves twelve crystallographic cages with an inner diameter of $\sim$0.4 nm, and two free O^{2-} ions accommodated in two cages out of the twelve cages. Most of the functionalities derived from C12A7 are realized by replacing the free O^{2-} ions with active anion species such as O^-, O_2^-, H^-, and electrons [9–11,13,14]. For instance, with an incorporation of H^- ions in the cages and illumination of ultraviolet (UV) light, the insulating C12A7 is converted to a persistent electronic semiconductor. The electrical conductivity is induced by the generation of mobile electrons, which are released from the H^- ions. Further, high-density mobile electrons are generated by removing the free O^{2-} ions by several routes [11,15,16] such as thermally annealing C12A7 with Ti metal at $\sim$1100 °C. The electron-doped C12A7 (C12A7:e^-) exhibits a low work function of 2.4 eV [17] as well as an insulator-metal transition [15] by increasing the electron concentration. Moreover, the maximum electron-doped C12A7 undergoes a superconducting transition at $\sim$0.2 K [18]. Such features make C12A7 very attractive as an electronic active material, and fabrication of a high-quality film is crucial for developing its applications.

To systematically investigate the materials properties and to extend potential applications, it is important to develop new isostructural materials. However, probably due to the unusual crystal structure, there has been no report of an isostructural crystal except $12SrO \cdot 7Al_2O_3$ (S12A7), whose syntheses were reported by Yamaguchi et al. using a sol–gel method [19] and Hayashi et al. using a solid-phase reaction [20]. S12A7 has a larger lattice constant (a=1.233 nm) than that of C12A7 (a=1.199 nm), and thus larger cages. Therefore, we expect that S12A7 may accommodate larger active anions than C12A7 does, and the uptake and release of the encaged anions would occur more easily.

In previous studies, we have reported fabrication of polycrystalline thin films of C12A7 and S12A7 on MgO (001) single-crystal substrates [21,22]. In this paper, we succeeded in growing hetero-epitaxial thin films of C12A7 and S12A7. We chose

* Corresponding author. Fax: +81 45 924 5127, 81 29 860 4674 .
E-mail addresses: m-miyakawa@lucid.msl.titech.ac.jp, MIYAKAWA.Masashi@nims.go.jp (M. Miyakawa).
[1] Present address: Superconducting Materials Center, National Institute for Materials Science, 1-1 Namiki, Tsukuba, Ibaraki 305-0044, Japan.

0022-4596/$ - see front matter © 2009 Elsevier Inc. All rights reserved.
doi:10.1016/j.jssc.2009.11.031

$Y_3Al_5O_{12}$ (YAG) as a substrate because the basic crystal structure of C12A7 is similar to that of YAG except for the cage structure and the free O^{2-} ions and, therefore, the lattice mismatch is as small as −0.1%. This paper also provides electron transport properties in C12A7 and S12A7 measured on electron-doped epitaxial films. The electron-doped films exhibited metallic conduction both for C12A7 and S12A7 films when the electron concentration exceeded $1\times10^{21}\,cm^{-3}$. In a S12A7/C12A7 double-layered film, an enhancement in the electron mobility was observed, which may originate from structural improvement of the S12A7 epitaxial layer due to the presence of C12A7 buffer layer and/or electron accumulation at the S12A7/C12A7 interface.

2. Method

2.1. Film growth and electron doping

The epitaxial thin films of stoichiometric C12A7 were fabricated on YAG (001) and (110) single-crystal substrates (Furuuchi Chemical Corporation) by a combined method of pulsed laser deposition (PLD) and post-deposition thermal crystallization. Amorphous C12A7 (a-C12A7) films were deposited at room temperature (RT) in a pure O_2 gas with a pressure of ~2.3 Pa using an ArF excimer laser (193 nm, 10 Hz, $\sim3\,Jcm^{-2}$) for the excitation source and a sintered disk of stoichiometric C12A7 for the ablation target. Then, the a-C12A7 films were subjected to post-deposition annealing at 1150 °C for 1 h in a wet O_2 gas passed through a humidifier for crystallization. For comparison, non-oriented polycrystalline C12A7 films were fabricated on MgO (001) single-crystal substrates and subjected to crystallization at 1100 °C for 1 h in air [21].

For S12A7, we could not obtain an epitaxial film of S12A7 by several methods including the above method and direct deposition at high temperatures. Finally, we found that epitaxial S12A7 films were grown pseudo-homoepitaxially on the epitaxial films of C12A7. The a-S12A7 films were deposited using the PLD method at RT using an ArF excimer laser and a target of a S12A7 green pellet, which was obtained by a solid state reaction of γ-Al_2O_3 with $Sr(OH)_2\cdot8H_2O$ [20] and a subsequent cold iso-static pressing. An O_2 gas was introduced to the PLD chamber at a partial pressure of $\sim1\times10^{-3}$ Pa during the deposition. The a-S12A7 films were subjected to post-annealing treatments for crystallization at 700–950 °C for 1 h in a wet O_2 gas. Note that the introduction of H_2O or H_2O-related species is the key for obtaining the crystalline C12A7 and S12A7 phases as known in previous reports on synthesis of bulk C12A7 [1] and S12A7 [20]. For example, Hayashi et al. [20] reports that the presence of Sr-hydrogarnet precursors plays crucial roles in the formation of S12A7, and, indeed, we could not obtain the crystalline S12A7 phase by post-annealing a-S12A7 films in a dry O_2 gas.

Unlikely conventional semiconductors, high-density mobile electrons are doped to C12A7 by removing the free O^{2-} ions as reported in Ref. [11], which leaves electrons in the cages so as to keep the charge neutrality of the crystal lattice. In this study, the free O^{2-} ions were removed by a reduction treatment reported in Ref. [16], in which oxygen-deficient amorphous C12A7 layers were deposited on the C12A7/S12A7 films at ~750 °C for C12A7 and ~650 °C for S12A7 in vacuum ($<\sim10^{-4}$ Pa) in order to extract the free O^{2-} ions from the bottom films. The top amorphous C12A7 layer was removed by mechanical polishing before the electrical measurements.

2.2. Characterization

The film thicknesses were measured by grazing-angle X-ray reflectivity spectroscopy (see Supplemental Figure S1 for examples). Crystal structures of the films were identified by X-ray diffraction (XRD) measurements with the Bragg–Brentano optics configuration (Rigaku, RINT2500, Cu$K\alpha$). A high-resolution X-ray diffraction (HR-XRD) (RIGAKU ATX-G, Cu $K\alpha_1$) apparatus was also used for determining crystallite orientations and for characterizing the film crystallinity. Out-of-plane (ω-coupled 2θ scan), in-plane (ϕ-coupled $2\theta\chi$ scan) HR-XRD patterns and reciprocal space maps were measured at RT to determine epitaxial relationships among the C12A7 film, the S12A7 film and the YAG substrate. Optical transmission and reflection spectra from UV to near infrared region (NIR) were measured at RT using a conventional spectrophotometer (Hitachi U4000). The internal absorption coefficients α_i were evaluated using $\alpha_i=-\ln[T/(1-R)]/d$, where T is the measured transmittance, R the reflectance, and d the film thickness. Electrical resistivity measurements were carried out with a standard four-probe method at temperatures of 2–305 K using a physical property measurement system (PPMS, Quantum Design). Carrier concentrations were evaluated at RT from Hall voltage measurements using a van der Pauw configuration [23].

3. Results and discussion

3.1. Structure, optical and electrical properties of C12A7 epitaxial film

Figs. 1a and b show the out-of-plane HR-XRD patterns of the as-crystallized (i.e., undoped) C12A7 thin film on YAG (001). Only the sharp diffraction peaks assignable to the C12A7 00l and the YAG 00l diffractions were observed as shown in Fig. 1a. Fig. 1b shows a magnified view around the diffraction at 29.6°, which show clear and separated peaks assigned to YAG 004 and C12A7 004 diffractions. Similar separated peaks are observed also for the 008 diffraction at 62°. These results indicate that the C12A7 film is selectively oriented along the 〈001〉 direction. The full width at half maximum (FWHM) of a C12A7 004 rocking curve is as small as ~0.02° (72 arcsec) (inset), which is comparable to that of a single-crystal grown by the Czochralski method (96 arcsec [24]). Because the lattice parameters of C12A7 and YAG are very similar, the in-plane diffraction peaks were not separately observed and the in-plane orientation was not determined. Therefore, we measured the reciprocal space map around the 408 diffractions of YAG and C12A7 (Fig. 1c). Clear diffractions from the C12A7 film and the YAG substrate are observed, and their ϕ scan curves (Fig. 1d) show that they have a four-fold symmetry corresponding to the cubic symmetry of C12A7 and YAG crystals, indicating that the film is oriented also in-plane. These results substantiate that the film crystallizes hetero-epitaxially on the YAG (001) substrate with the orientation relationship of (001)[100] C12A7 || (001)[100] YAG. The lattice parameters estimated from Fig. 1 are a=1.201 nm and c=1.206 nm. It was also confirmed that (110)-oriented C12A7 epitaxial films were crystallized on YAG (110) surfaces by the same procedure, which had the same lattice parameters within experimental distribution/errors (<0.001 nm in lattice parameter).

Fig. 2a shows the optical absorption spectra of the C12A7 films (the film thickness was ~80 nm) before and after the electron doping. The as-crystallized (i.e., undoped) C12A7 films were electrically insulating and did not exhibit a peak structure in the absorption spectra. After the electron doping, the C12A7 films became conductive with the RT resistivity (ρ_{RT}) of $\sim1.2\times10^{-3}\,\Omega$cm, which simultaneously induced two absorption bands in the NIR region < 1.5 eV and the visible region around ~2.7 eV. These are respectively assigned to free carrier absorption (i.e., intraband transition) by the doped electrons and interband transition of the doped electrons [25,26]. These

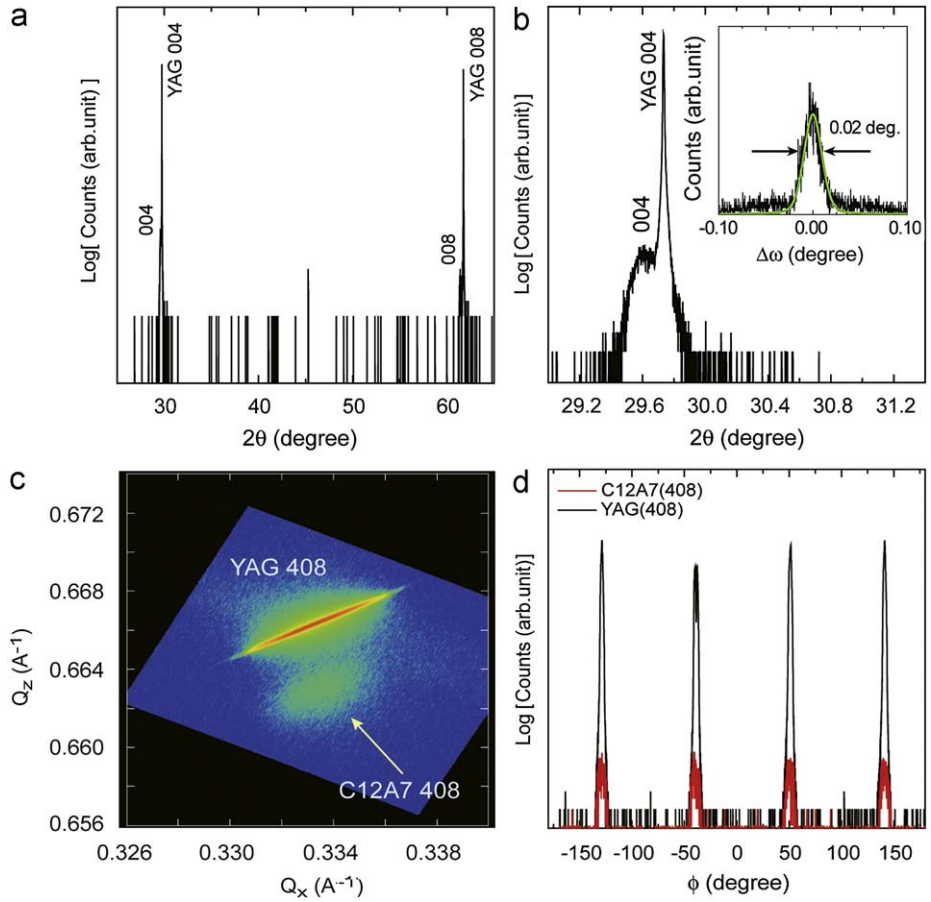

Fig. 1. HR-XRD patterns of the as-crystallized C12A7 thin films on YAG (001) single-crystal substrate. (a) Out-of-plane pattern and (b) a magnified view around the 004 diffractions. Inset in (b) shows the out-of-plane rocking curve (ω scan) of the C12A7 004 diffraction. (c) Reciprocal space map around the 408 diffractions, and (d) the ϕ scans of the 408 diffractions.

observations substantiate that the reduction treatment by the oxygen-deficient a-C12A7 layer actually generates mobile electrons in the cages. Fig. 2b shows the temperature (T) dependences of ρ of the C12A7:e$^-$ epitaxial and the non-oriented polycrystalline films. The ρ value increases as T increases, showing metallic conduction (i.e., the slopes dρ/dT are positive). The ρ was smaller and its slope was larger for the epitaxial film than those of the non-oriented C12A7:e$^-$ film on MgO (001). It implies that the carrier transport properties are improved in the epitaxial film, which will further be discussed below. Fig. 2c shows the temperature dependences of the electron mobility (μ_H) and concentration ($N_{e,Hall}$) obtained from the Hall measurements, where those for the non-oriented C12A7:e$^-$ film are also shown for comparison. For the C12A7:e$^-$ epitaxial film, the $N_{e,Hall}$ value ($\sim 1.9\times10^{21}\,cm^{-3}$) at RT is independent of temperature while μ_H decreases from $\sim$11 to $\sim 3\,cm^2(Vs)^{-1}$ with increasing T. Similar temperature dependences are observed also for the non-oriented C12A7:e$^-$ film. The $\mu_H(T)$ follows a $T^{-0.25}$ dependence for the non-oriented film while a $T^{-0.65}$ dependence is observed for the epitaxial film. The former $T^{-1/4}$ dependence implies that the electron transport would be controlled by grain boundary potential barriers through a percolation conduction [27,28]. On the other hand, the latter is close to a T^{-1} dependence, which is interpreted as phonon scattering in a metallic conductor. It suggests that the crystalline quality in the epitaxial films is improved from that of the non-oriented film. Fig. 2d shows the variation of $N_{e,Hall}$ against the optical absorption coefficient at 2.7 eV ($\alpha_{i2.7}$, i.e., at the peak energy of the visible absorption in Fig. 2a) for the C12A7:e$^-$ films that exhibit metallic conduction. It shows a good linear correlation, supporting the previous result [26] that $\alpha_{i2.7}$ is directly associated with the concentration of the mobile electrons (N_e). Also, we have observed similar correlation between the concentration of the encaged electrons obtained by ESR measurements and $\alpha_{i2.7}$ for low conductive C12A7:e$^-$ [11], in which hopping conduction governs the electron transport, without showing definite Hall voltages. These results guarantee that N_e is estimated from the $\alpha_{i2.7}$ value even for samples that do not give definite Hall voltages and in which hopping conduction controls the electron transport.

3.2. *Effects of C12A7 epitaxial layer on epitaxial growth of S12A7 film*

Fig. 3a shows the out-of-plane XRD patterns of the as-crystallized S12A7 films fabricated directly on a YAG (001) substrate and on a C12A7 (001) epitaxial film on a YAG (001) substrate. Several diffraction peaks arising from different planes are observed for the film without a C12A7 epitaxial layer (upper pattern), which indicates the film is non-oriented even when it was crystallized on the single-crystalline YAG (001) substrate. On the other hand, the film grown on the C12A7 epitaxial film (lower pattern) exhibits 00l diffractions only, indicating the film grows preferentially along the $\langle 00l \rangle$ direction (c-axis). With increasing the annealing temperature from 700 to 950 °C, the peak position

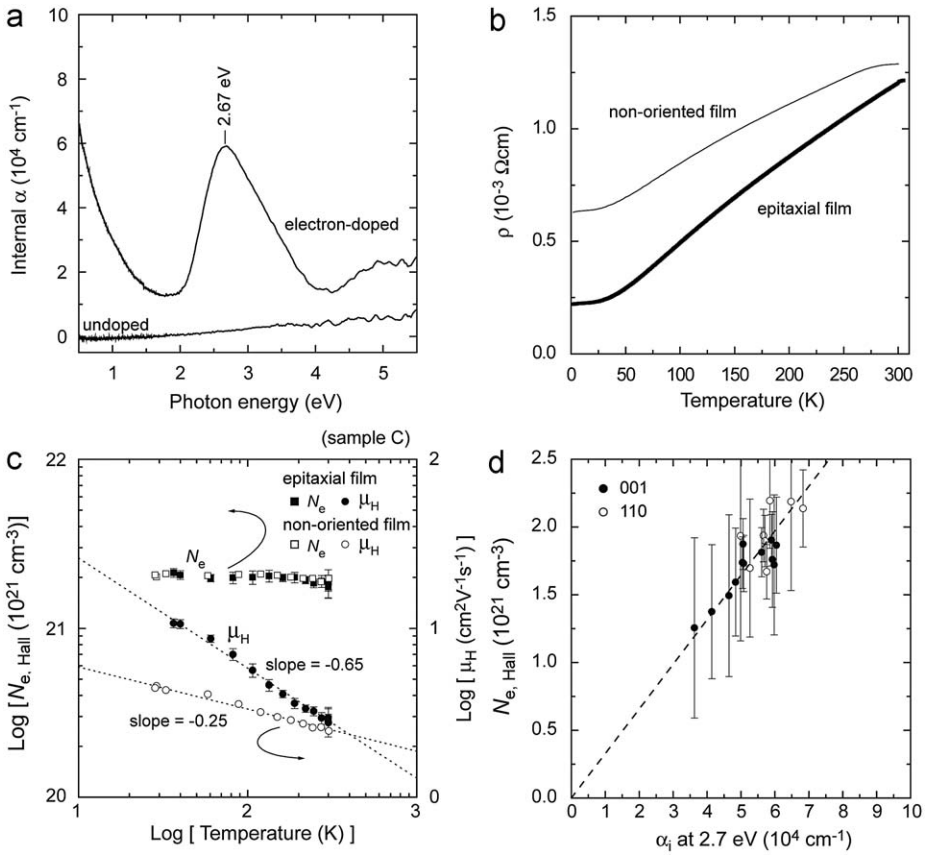

Fig. 2. Optical and electrical properties of as-crystallized (undoped) and electron-doped C12A7 epitaxial thin films on YAG (001) single-crystal substrates. Those of non-oriented polycrystalline C12A7 films are also shown in Figs. b and c for comparison. (a) Optical internal absorption spectra of the undoped and the electron-doped C12A7 epitaxial films at RT. (b) ρ–T curves in the temperature range of 2–305 K, and (c) temperature dependences of $N_{e,Hall}$ and μ_H in the temperature range of 35–300 K. (d) Relationship between the $N_{e,Hall}$ at RT and the optical internal absorption coefficient α_i at ~2.7 eV.

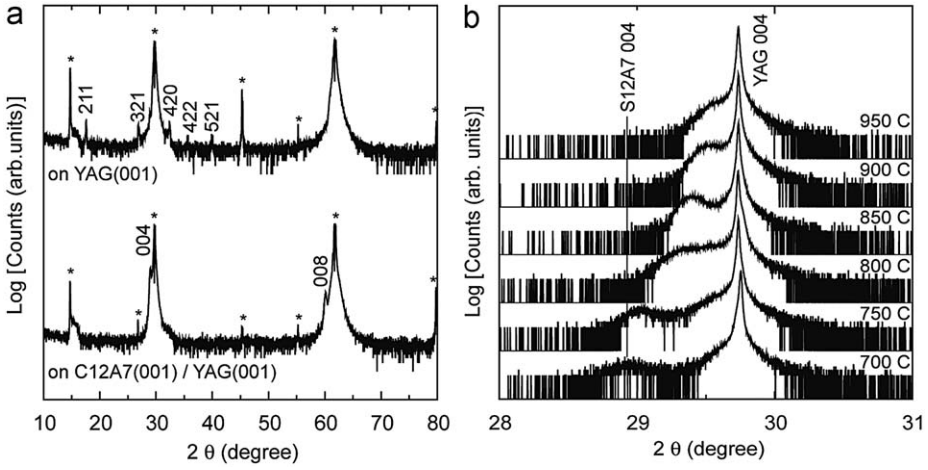

Fig. 3. Out-of-plane XRD patterns of as-crystallized S12A7 films. (a) XRD patterns for S12A7/YAG (001) film (upper) and S12A7/C12A7/YAG (001) film (lower). The asterisks indicate diffractions from the YAG substrate. (b) Annealing temperature dependence of the HR-XRD patterns of S12A7/C12A7 double-layered films.

of the 004 diffraction shifted to larger angles and the lattice parameter decreases for the S12A7 films on C12A7/YAG as shown in Fig. 3b (detail will be discussed in the next section). It suggests that a solid-phase reaction of S12A7 with the C12A7 layer occurs and produces solid-solutions of S12A7 and C12A7 at the higher temperatures. Therefore, we, hereafter, fixed the annealing temperature at 750 °C for growing the S12A7 epitaxial films on C12A7.

3.3. Structure, optical and electrical characterization of S12A7/C12A7 double-layered film

Fig. 4a shows an out-of-plane HR-XRD pattern of the S12A7/C12A7 film on a YAG substrate after the crystallization at 750 °C. It reveals the film is oriented along the *c*-axis. A magnified view around the 004 diffraction (Fig. 4b) shows that the diffraction peak is composed of three 004 diffractions assigned

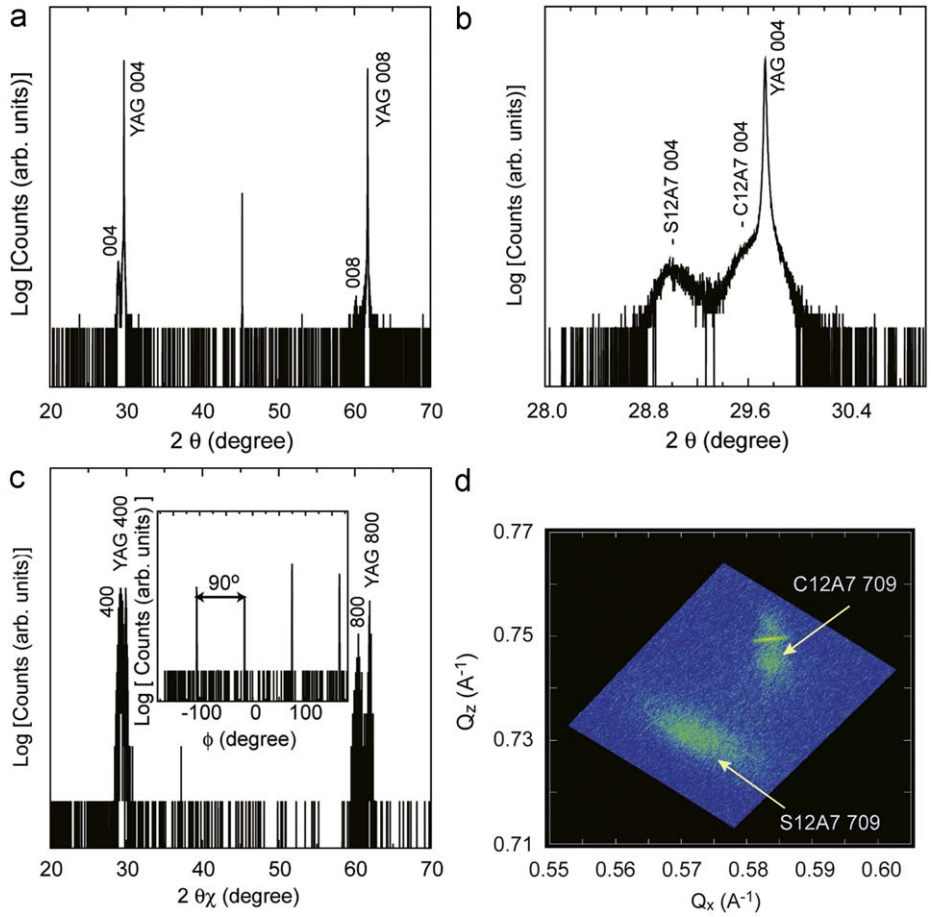

Fig. 4. HR-XRD patterns of as-crystallized S12A7/C12A7 film. (a) Out-of-plane pattern and (b) a magnified view around the 004 diffraction. (c) In-plane pattern. The inset shows the ϕ scan of the 400 diffraction. (d) Reciprocal space map around the 709 diffractions. Note that a very sharp and intense diffraction peak at Q_x=0.585 Å^{-1}, Q_z=~0.750 Å^{-1} is from a YAG substrate.

to S12A7, S12A7, and YAG. A similar orientation relationship is observed also in the in-plane HR-XRD pattern (Fig. 4c), in which only the *h*00 diffractions are observed. Further, the ϕ scan of the S12A7 400 diffraction (inset) exhibits a four-fold symmetry resulting from the cubic crystal lattice, which indicates that the orientation relationship of the S12A7 film to the YAG substrate is the same as that to the C12A7 film. To obtain further information on the orientation relationship, a reciprocal space map of the asymmetric (709) plane was measured (Fig. 4d). Two diffractions arising from the S12A7 and C12A7 films are observed. Moreover, the four-fold symmetry was also confirmed from the ϕ scans of these diffractions. These observations lead to the conclusion that the S12A7 film is grown hetero-epitaxially on the C12A7/YAG substrate with the orientation relationship of (001)[100] S12A7 || (001)[100] C12A7 || (001)[100] YAG. The lattice parameters, *a* and *c*, of the S12A7 film, are respectively, estimated to be *a*=1.225 nm and *c*=1.230 nm from the peak positions of the 800 and 008 diffractions, which correspond to −0.6% and −0.2% reduction from the lattice parameters of bulk S12A7. The smaller *a*-axis length indicates that the crystal lattice in the S12A7 film is locked by that of the bottom C12A7 layer with the smaller lattice parameter.

Fig. 5a shows the optical internal absorption spectra of the as-crystallized (undoped) and electron-doped S12A7/C12A7 (S12A7:e$^-$/C12A7:e$^-$) films. Those of non-oriented S12A7:e$^-$ (the dashed line) and the epitaxially-grown C12A7:e$^-$ films (the dotted line) are also shown for comparison. The overall profile of the absorption spectrum of the S12A7:e$^-$/C12A7:e$^-$ film resembled those of the non-oriented S12A7:e$^-$ and the C12A7:e$^-$ epitaxial films. Two absorption bands are induced in the NIR region < ~1.5 eV and the visible region around ~2.5 eV as a result of the electron doping. As stated above, these absorption bands are associated with the intraband transition (in the NIR region) and the interband transition (at ~2.5 eV) of the mobile electrons doped in the cages [25,26]. The peak position of the ~2.5 eV band is lower for S12A7:e$^-$/C12A7:e$^-$ than that of the C12A7:e$^-$ due likely to the larger cage size of S12A7 than that of C12A7. It should be noticed that the optical spectrum of the S12A7:e$^-$/C12A7:e$^-$ film should comprise those of S12A7:e$^-$ and C12A7:e$^-$, which is actually confirmed by the fact that the spectrum shapes of the non-oriented S12A7:e$^-$ film, the C12A7:e$^-$ epitaxial film, and the S12A7:e$^-$/C12A7:e$^-$ double-layered film are systematically varied. It further indicates that mobile electrons are doped both to the S12A7 layer and the C12A7 layer in the S12A7/C12A7 double-layered film.

We analyzed the electron concentrations (N_e) in the S12A7 and the C12A7 layers separately from the absorption spectrum of the S12A7:e$^-$/C12A7:e$^-$ film, $\alpha_{obs}(h\nu)$. Because the S12A7:e$^-$ and C12A7:e$^-$ layers are stacked in series, $\alpha_{obs}(h\nu)$ is expressed by

$$\alpha_{obs}(h\nu)\cdot(d_S+d_C)=[\alpha_S(h\nu)\cdot d_S+\alpha_C(h\nu)\cdot d_C], \quad (1)$$

where $\alpha_S(h\nu)$ and $\alpha_C(h\nu)$ are the absorption coefficients of S12A7:e$^-$ and C12A7:e$^-$, and d_S and d_C the thickness' of the S12A7:e$^-$ and C12A7:e$^-$ layers, respectively. Here, we took the $\alpha_S(h\nu)$ and $\alpha_C(h\nu)$ spectra from those measured on the single-layered non-oriented S12A7:e$^-$ film and C12A7:e$^-$ epitaxial film,

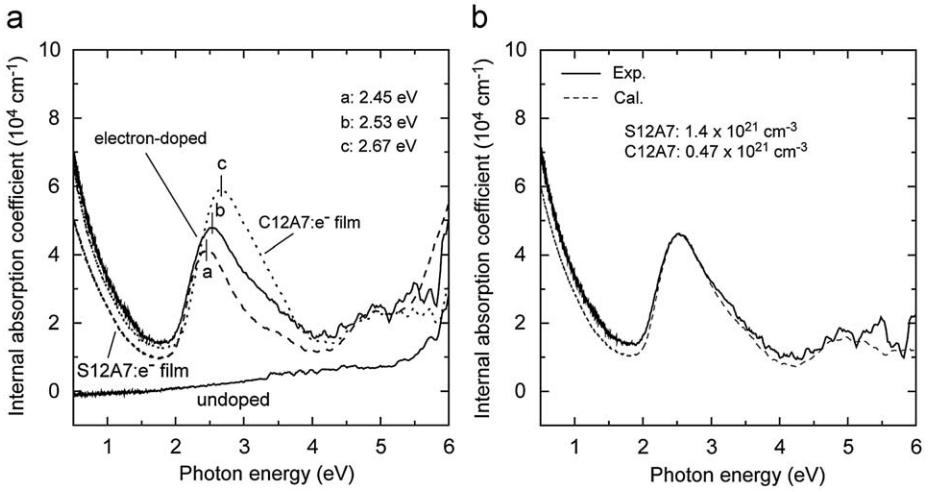

Fig. 5. Optical absorption spectra of S12A7/C12A7 films. (a) Internal absorption spectra of undoped (as-crystallized) and electron-doped films. Those for the non-oriented S12A7:e$^-$ (S12A7:e$^-$ film) and the C12A7:e$^-$ epitaxial films (C12A7:e$^-$ film) are also shown for comparison. (b) Experimental (solid line) and fitted (dashed line) absorption spectra.

respectively, which are shown in Fig. 5a. Since the α values at 2.7 eV is proportional to N_e as seen in Fig. 2d, Eq. (1) is re-written as

$$\alpha_{obs}(h\nu)\cdot(d_S+d_C)=[N_{e,S}C_S(h\nu)\cdot d_S+N_{e,C}C_C(h\nu)\cdot d_C], \quad (2)$$

where $N_{e,S}$ and $N_{e,C}$ are the electron concentrations in the S12A7:e$^-$ and C12A7:e$^-$ layers, and $C_S(h\nu)$ and $C_C(h\nu)$ are the proportional constants defined by $\alpha_C(h\nu)=C_C(h\nu)\cdot N_{e,C}$ and $\alpha_S(h\nu)=C_S(h\nu)\cdot N_{e,S}$. The d_S and d_C, were respectively, estimated to be 40.3 and 43.5 nm by grazing-angle X-ray reflectivity spectroscopy, and $N_{e,S}$ and $N_{e,C}$ were optimized by the least-squares method so as to reproduce the 2.7 eV absorption band of the $\alpha_{obs}(h\nu)$ spectrum.

Fig. 5b shows that the calculated spectrum reproduces well the observed absorption spectrum, which provided the fitted values of $N_{e,S}=1.4\times10^{21}$ and $N_{e,C}=0.47\times10^{21}\,cm^{-3}$. This result, the three times larger $N_{e,S}$ than $N_{e,C}$, indicates that the reduction treatment is more effective for the upper S12A7 layer and/or the electrons doped in the C12A7 layer were transferred to the S12A7 layer, which we will discussed again later.

Fig. 6 shows the temperature dependences of ρ for the S12A7:e$^-$/C12A7:e$^-$ film. Those of the non-oriented S12A7:e$^-$ and C12A7:e$^-$ epitaxial films are also shown. The ρ value of the double-layered film was $3.3\times10^{-3}\,\Omega$cm at RT, which is lower than that of the non-oriented S12A7:e$^-$ film ($\sim3.7\times10^{-3}\,\Omega$cm), suggesting an improvement of the crystalline quality in the epitaxial film compared to the non-oriented one. The S12A7:e$^-$/C12A7:e$^-$ double-layered film exhibits metallic type conduction although the slope of the ρ–T curves (dρ/dT) is small. This result suggests that the critical N_e value for insulator-metal transition in S12A7 is less than the $N_{e,S}$ value of $1.4\times10^{21}\,cm^{-3}$ and would be similar to that for C12A7 ($\sim1\times10^{21}\,cm^{-3}$). Hall voltage measurements revealed the apparent Hall mobility and sheet carrier density of the S12A7:e$^-$/C12A7:e$^-$ double-layered film were $1.9\,cm^2(Vs)^{-1}$ and $8.4\times10^{15}\,cm^{-2}$, respectively. The sheet carrier density is in good agreement with that estimated from the value obtained by the optical analysis ($N_{e,S}d_S+N_{e,C}d_C=7.7\times10^{15}\,cm^{-2}$), further supporting the validity of these analyses.

It should be noted that the ρ values of the S12A7:e$^-$/C12A7:e$^-$ double-layered film are one order of magnitude larger than those of the C12A7:e$^-$ epitaxial film. It resulted largely from the smaller N_e value ($0.92\times10^{21}\,cm^{-3}$ for the S12A7:e$^-$/C12A7:e$^-$ film (the average value) and $1.9\times10^{21}\,cm^{-3}$ for the C12A7:e$^-$ epitaxial film). Here, we like to point out that the observed apparent Hall

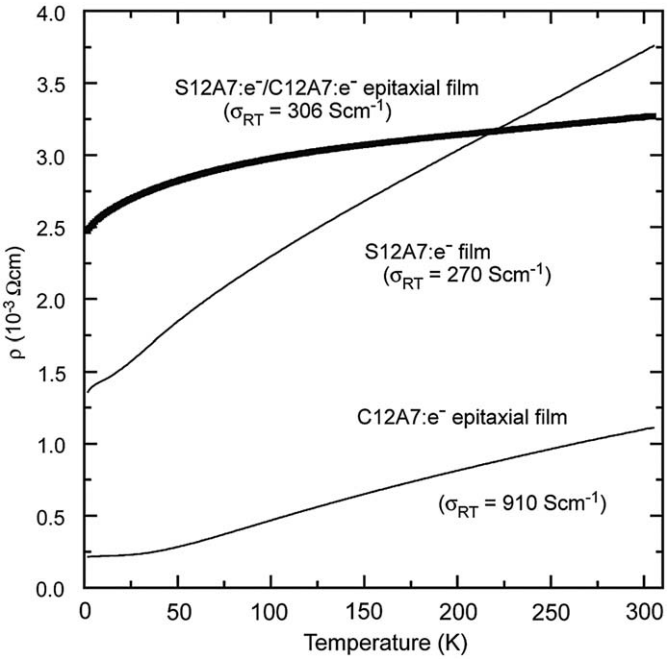

Fig. 6. Electrical resistivities of S12A7:e$^-$/C12A7:e$^-$ double-layered film as a function of temperature. Those for the non-oriented S12A7:e$^-$ and the C12A7:e$^-$ epitaxial films are also shown for comparison.

mobility of $1.9\,cm^2(Vs)^{-1}$ is not explained simply from the Hall mobilities of S12A7:e$^-$ and C12A7:e$^-$. Assuming a simple additive property for the observed sheet conductance S_{obs},

$$S_{obs}=S_{S12A7}+S_{C12A7} \quad (3)$$

is obtained, where S_{S12A7} and S_{C12A7} are the sheet conductances of the S12A7:e$^-$ and C12A7:e$^-$ layers, respectively. Using the mobilities and the sheet carrier densities obtained above, we obtain the relation $5.6\mu_{S12A7}+2.0\mu_{C12A7}=1.9\times7.7$ S. If we employ the observed values of $\mu_{C12A7}=1.06\,cm^2(Vs)^{-1}$, $\mu_{S12A7}=2.2\,cm^2(Vs)^{-1}$ is obtained. This value is doubly larger than that of the non-oriented S12A7:e$^-$ film with a similar N_e of $1.4\times10^{21}\,cm^{-3}$ ($1.2\,cm^2(Vs)^{-1}$ [22]) and even larger than that of a C12A7:e$^-$ bulk single-crystal ($\sim1.4\,cm^2(Vs)^{-1}$, which is estimated for the same N_e value) [15]. It would be explained by two

models. A simpler model would be that the structural improvement of the S12A7 epitaxial layer owing to the presence of the C12A7 buffer layer resulted in a smaller carrier scattering. We, however, consider that it alone cannot explain the mobility enhancement because the obtained mobility is larger than that of the C12A7:e^- bulk single-crystal. The other model is that there is a high mobility layer formed in the S12A7:e^-/C12A7:e^- film. It would be possible that the electron transfer from the C12A7:e^- layer to the S12A7:e^- layer occurs and forms an electron accumulation layer at the interface. As discussed above, the optical absorption analysis results provided the larger N_e in the S12A7:e^- layer, supporting this model. Such mobility enhancement originating from a two-dimensional interface would be interesting for realizing novel oxide electronic devices, which is similar to "high-electron mobility transistor (HEMT)" in compound semiconductor electronics [29,30].

4. Summary

Hetero-epitaxial crystallizations of C12A7 thin films are demonstrated using the lattice-mached substrate, YAG single-crystal, and the combined method of RT deposition by PLD and post-crystallization at 1150 °C in moisture oxygen. Further, pseudo-homoepitaxial growth of S12A7 films is also achieved on the C12A7 (100) epitaxial films by a similar method. Electron doping by the reduction treatment converted these films to metallic conductors with $\rho = \sim 1.2 \times 10^{-3}\,\Omega\,\mathrm{cm}$ for the C12A7:e^- film and $\rho = \sim 3.3 \times 10^{-3}\,\Omega\,\mathrm{cm}$ for the S12A7:e^-/C12A7:e^- film at RT. Optical analyses and Hall measurements revealed that the S12A7:e^- layer has three times larger electron concentration than that in the C12A7:e^- layer and suggested that a high-mobility layer is formed in the S12A7:e^-/C12A7:e^- double-layered film.

Acknowledgments

This study was supported by the Science and Technology Project for Element Strategy and a Grant-in-Aid for Scientific Research (S) from the MEXT, Japan.

Appendix A. Supplementary material

Supplementary data associated with this article can be found in the online version at doi:10.1016/j.jssc.2008.11.011.

References

[1] H.F.W. Taylor, Cement Chemistry, second ed., Thomas Telford, London, 1997.
[2] R.W. Nurse, J.H. Welch, A.J. Majumdar, Trans. Br. Ceram. Soc. 64 (1965) 323–332.
[3] J.A. Imlach, L.S.D. Glasser, F.P. Glasser, Cem. Concr. Res. 1 (1971) 57–61.
[4] G.I. Zhmoidin, A.K. Chatterjee, Cem. Concr. Res. 14 (1984) 386–396.
[5] P.P. Williams, Acta Cryst. B 29 (1973) 1550–1551.
[6] Q.-L. Feng, F.P. Glasser, R. Alan-Howie, E.E. Lachowski, Acta Cryst. C 44 (1988) 589–592.
[7] J.T.S. Irvine, A.R. West, Solid State Ionics 40/41 (1990) 896–899.
[8] K. Hayashi, P.V. Sushko, D.M. Ramo, A.L. Shluger, S. Watauchi, I. Tanaka, S. Matsuishi, M. Hirano, H. Hosono, J. Phys. Chem. B 111 (2007) 1946–1956.
[9] K. Hayashi, M. Hirano, S. Matsuishi, H. Hosono, J. Am. Chem. Soc. 124 (2002) 738–739.
[10] K. Hayashi, S. Matsuishi, T. Kamiya, M. Hirano, H. Hosono, Nature 419 (2002) 462–465.
[11] S. Matsuishi, Y. Toda, M. Miyakawa, K. Hayashi, T. Kamiya, M. Hirano, I. Tanaka, H. Hosono, Science 301 (2003) 626–629.
[12] H. Bartl, T. Sceller, Neues. Jahrb. Mineral. Monatsh. 35 (1970) 547–552.
[13] K. Hayashi, S. Matsuishi, M. Hirano, H. Hosono, J. Phys. Chem. B 108 (2004) 8920–8925.
[14] M.I. Bertoni, T.O. Mason, J.E. Medvedeva, A.J. Freeman, K.R. Poeppelmeier, B. Delley, J. Appl. Phys. 97 (2005) 103713-1–103713-6.
[15] S.W. Kim, S. Matsuishi, T. Nomura, Y. Kubota, M. Takata, K. Hayashi, T. Kamiya, M. Hirano, H. Hosono, Nano Lett. 7 (2007) 1138–1143.
[16] M. Miyakawa, M. Hirano, T. Kamiya, H. Hosono, Appl. Phys. Lett. 90 (2007) 182105-1–182105-3.
[17] Y. Toda, H. Yanagi, E. Ikenaga, J.J. Kim, M. Kobata, S. Ueda, T. Kamiya, M. Hirano, K. Kobayashi, H. Hosono, Adv. Mater. 19 (2007) 3564–3569.
[18] M. Miyakawa, S.-W. Kim, H. Hirano, Y. Kohama, H. Kawaji, T. Atake, H. Ikegami, K. Kono, H. Hosono, J. Am. Chem. Soc. 129 (2007) 7270–7271.
[19] O. Yamaguchi, A. Narai, K. Shimizu, J. Am. Ceram. Soc. 69 (1986) C-36.
[20] K. Hayashi, N. Ueda, S. Matsuishi, M. Hirano, T. Kamiya, H. Hosono, Chem. Mater. 20 (2008) 5987–5996.
[21] M. Miyakawa, K. Hayashi, M. Hirano, Y. Toda, T. Kamiya, H. Hosono, Adv. Mater. 15 (2003) 1100–1103.
[22] M. Miyakawa, N. Ueda, T. Kamiya, M. Hirano, H. Hosono, J. Ceram. Soc. Jpn. 115 (2007) 567–570.
[23] The errors of the resistivity and the Hall voltage measurements were respectively $< 2\%$ and $< 12\%$ for the C12A7:e^- films, and $< 2\%$ and $< 20\%$ for the S12A7/C12A7:e^- double-layered film.
[24] K. Kurashige, Y. Toda, S. Matstuishi, K. Hayashi, M. Hirano, H. Hosono, Cryst. Growth & Des. 6 (2006) 1602–1605.
[25] P.V. Sushko, L.S. Alexander, K. Hayashi, M. Hirano, H. Hosono, Phys. Rev. Lett. 91 (2003) 126401.
[26] S. Matsuishi, S.W. Kim, T. Kamiya, M. Hirano, H. Hosono, J. Phys. Chem. C 112 (2008) 4753–4760.
[27] D. Adler, L.P. Flora, S.D. Senturia, Solid State Commun. 12 (1973) 9–12.
[28] K. Nomura, H. Ohta, K. Ueda, T. Kamiya, M. Hirano, H. Hosono, Appl. Phys. Lett. 85 (2004) 1993–1995.
[29] R. Dingle, H.L. Störmer, A.C. Gossard, W. Wiegmann, Appl. Phys. Lett. 33 (1978) 665–667.
[30] T. Mimura, S. Hiyamizu, T. Fujii, K. Nanbu, Jpn. J. Appl. Phys. 19 (1980) L225–L227.